Research on Micro-Turbine Operating State Characterization Based on Bearing Vibration Signals Analysis

Ning Li

School of Mechanical Engineering, Dalian University of Technology, Dalian, 116024, China.
E-mail: lining02@mail.dlut.edu.cn

Xiaowei Wang and Tongguang Yang

School of Mechanical Engineering and Automation, Northeastern University, Shenyang, 110819, China.

Qingkai Han

School of Mechanical Engineering, Dalian University of Technology, Dalian, 116024, China.
School of Mechanical Engineering and Automation, Northeastern University, Shenyang, 110819, China.

(Received 4 July 2023; accepted 9 October 2023)

An air flow-driven micro-turbine, widely used in air-condition control systems in aircraft cabins, train coaches, etc., exhibits complex vibration behaviors under stable or unstable inlet flow conditions, and especially has a certain correlation with speeds. In this paper, the vibration responses of the micro-turbine undergoing stable and unstable inlet flows measured on a test rig are analyzed and compared by using different signal processing methods, which include time and frequency domain methods, and statistical and nonlinear methods. First, the test rig system of the airflow-driven micro-turbine, the instrument system and four typical experimental cases are introduced. Then the measured vibration signals are analyzed and compared by time domain characteristic parameters (peak-to-peak value, RMS value and kurtosis value), statistical parameters (auto-correlation and BDS), and amplitude spectra in the frequency domain, statistic spectrum indicators (SSI) based on Welch's periodogram of power spectra, and the spectra of selected IMF components based on Hilbert-Huang Transform (HHT). In particular, some nonlinear feature analyzing methods, including Pseudo-Poincare mapping diagrams and Lempel-Ziv(LZ) complexity, are also used for analyzing measured vibration responses. The obtained results using the above multiple methods are compared and show that, when the inlet flow of the turbine fluctuates significantly, the nonlinear characteristics of the turbine bearings are significantly higher than those of the relatively stable inlet flow and speed conditions. Under these circumstances, commonly used time-frequency analysis methods cannot characterize the different speed operating state of the turbine, and LZ-Complexity and other nonlinear characterization methods should be used to better understand the characteristics of different speeds under unstable conditions.This study provides references for the aerodynamic stability monitoring of the micro-turbine and its design improvement.

1. INTRODUCTION

Many airflow-driven micro-turbines are widely used in environmental control systems for cabins and inboard temperature control of civilian aircraft and passenger coaches of trains. As an example of micro-turbines with environmental control systems, a part of high-pressure air is induced from the compressor of an aeroengine for driving and heat exchange, in a practical operation process, under the given pressure ratio and rotor structure, the high-pressure airflow will lead to abnormal vibration of the micro-turbine, especially in the case of unstable inlet flow. The abnormal vibration behavior of the micro-turbine caused by unstable inlet flow will affect the impeller, bearing, connecting pipelines and other surrounding structures greatly, even causing rapid failure of the machine and other serious consequences.[1]

At present, it is recognized that the abnormal vibration of micro-turbines is directly harmful to air supply, temperature regulation, structural life, and reliability. Meanwhile, there are relatively few studies on the vibration of micro-turbines under different bleeding air conditions and rotational speeds, so it is necessary to conduct in-depth research. The research on aerodynamic performance and vibration of the micro-turbines can refer to the achievements in the field of compressors, and the representative research achievements are shown as follows.

Tian[2] analyzed dynamic characteristics of a floating offshore wind turbine under different wind speed and wave height. Chun[3] discovered the size of the vena and acceleration in the axial direction has an obvious relation with the discharge coefficient of gas turbines. Wei[4] proposed a numerical simulation of flow characteristic of aero engines under different rotating conditions. Liu[5] proposed a rolling bearing fault evolution state indicator based on deep convolutional neural network (CNN) and wavelet analysis of vibration signals. Fu[6] found the formation and development mechanism of the unsteady vortex flow in the vaneless space of pump-turbine and is associated with the distribution characteristic of the velocity field. Yoon[7] studied combustion instability based on the flame structure measurement technique under vibrational inlet air temperature.

A rotating stall and surging of the compressor are an unstable phenomenon under the condition of small flow rate, which limits the working performance. Inoue M et al.[8] found that the dynamic pressure signal fluctuates regularly at stabilization, and the regularity is destroyed near instability. Hendricks G J, et al.[9] found that the modal wave in the high-speed compressor has more high-frequency components than that in the low-speed compressor. Meng F X et al.[10] established the simulation model of a micro-turbine fan air circulator in an aircraft environmental control system. Song J X et al.[11] analyzed the dynamic performance of the air-entraining part of the environmental control system of a certain type of aircraft and conducted an experimental study. Zhao et al.[12] studied the pressure transient responses and temperature transient responses of the bleed system of an aircraft environmental control system when the inlet flow pressure and temperature was varied. Gu et al.[13] studied the stall and surge characteristics of flow instability in high rotating speeds centrifugal compressor by the experimental method.

The existing micro-turbine operating status analysis methods are limited by the acquisition location and method, making it difficult to accurately analyze the vibration characteristics of internal rotating shafts, bearings, and other components when the speed changes frequently. For micro-turbines that often operate in high-speed ranges, whether from the perspective of operating status monitoring or vibration noise control, it is necessary to obtain the internal vibration characteristics of micro turbines. Based on the analysis of bearing vibration signals, the operation status of the micro turbine can be directly obtained from the actual operating parameters inside the micro turbine. At the same time, there is no significant interference to the internal airflow field of the turbine.

Furthermore, the research on the abnormal vibration behavior of mechanical equipment is generally drawn on signal analysis and characterization methods. The representative achievements are reviewed as follows. The root mean square (RMS) can reflect the overall trend of bearing fault.[14] The kurtosis values are sensitive to aperiodic interference.[15] Jin et al.[16] proposed a novel fault diagnosis method that is based on radial basis function neural network with a power spectrum of the Welch method. Pei et al.[17] proposed a method for a rolling bearing fault feature extraction based on auto-correlation and energy operator enhancement. In addition, some distribution test methods of statistical analysis of data or signals can also be used to compare the unstable or nonlinear characteristics of mechanical vibration signals. For example, the BDS test which is exploited by Brock and Dechert is a non-parametric test for serial independence based on the correlation integral of the scalar series which asymptotically converges to a unit normal.[18] However, a few works of statistical analysis of the spectral content deal with the abnormal vibration characteristics of machines.[19] They developed an original method based on the statistical process of Welch's periodogram of the measured vibration signals to distinguish the machine's vibration states.[20] Modern signal analysis representation methods have been proposed such as Wigner Distribution,[21] Wavelet Transform,[22] Singular Value Decomposition,[23] Empirical Mode Decomposition,[24] Variational Mode Decomposition,[25] Hilbert-Huang Transform,[26] etc. Hilbert-Huang Transform (HHT) is an excellent time-frequency signal analysis method, especially suitable for nonlinear and non-stationary signal sequence processing.[27] Sun[28] analyses deformation and vibration of compressor rotor blades based on fluid-structure coupling.

In addition to multi-harmonics and stationary random signals, many stationary or non-stationary signals sometime exhibit nonlinear characteristics, which are difficult to distinguish from each other. Therefore, it is also very important to analyze the nonlinear characteristics of mechanical vibration signals. The main methods of signal nonlinear analysis include the Pseudo-Poincare mapping diagrams that are based on phase space reconstruction theory,[29] fractal,[30] Lempel-Ziv complexity[31,32] and other methods to describe the characteristics of sophisticated system behavior. Complexity reflects velocity of emergence of new patterns as the length of the series increases, which can quantitatively describe the state changes of the system.

This paper focuses on a comparison study of the vibration behavior of an airflow-driven micro-turbine with multiple characterization methods. In addition, it is based on the measured radial vibration responses of the micro-turbine exposed to stable or unstable inlet flows at different rotating speeds. Several signal processing methods are adopted, including time domain analysis, frequency domain analysis, time-frequency domain analysis, and nonlinear analysis. The main contributions are generalized as follows.

1. The time domain analyses; statistical analyses and frequency domain analyses are utilized. Time domain characteristic parameters (peak-to-peak value, RMS value and kurtosis value), statistical parameters (auto-correlation and BDS), and amplitude spectra in frequency domain, statistic spectrum indicators (SSI) are illustrated to compare with each other.

2. The spectra of selected IMF components based on HHT are adopted to analyze the vibration signals. The Phase analysis method is also used to compare the vibration signals under different cases. There are also obvious differences under four cases based on the above methods.

3. The vibration signals of the micro-turbine are calculated and compared quantitatively by nonlinear methods including the Pseudo-Poincare mapping diagrams based on the phase space reconstruction theory, and the LZ complexity values. These results are then compared and discussed.

2. EXPERIMENTAL DEVICE AND SCHEME SECTION

2.1. Experiment System

The airflow-driven micro-turbine consists of a compressor and turbine, which is connected by a rotating shaft with 2 bearings. The structure of the micro-turbine is shown in Fig. 1. Figure 1(a) is a cross-sectional view of the micro-turbine, and Fig. 1(b) is the principle of operation of the micro-turbine.

The experiment system is constituted of a turbine body, compressor, air tank, pipeline, inlet and outlet regulating valves, and mounting brackets, as shown in Fig. 2.

The operation of the micro-turbine system is as follows: first, start the compressor and run it for a period of time to deliver a certain amount of air to the storage aiming to reach certain pressure, and then open the valve of the micro-turbine's pipeline for bleeding air to drive the turbine. The general running time is about 2–10 minutes. With the reduction of air sup-

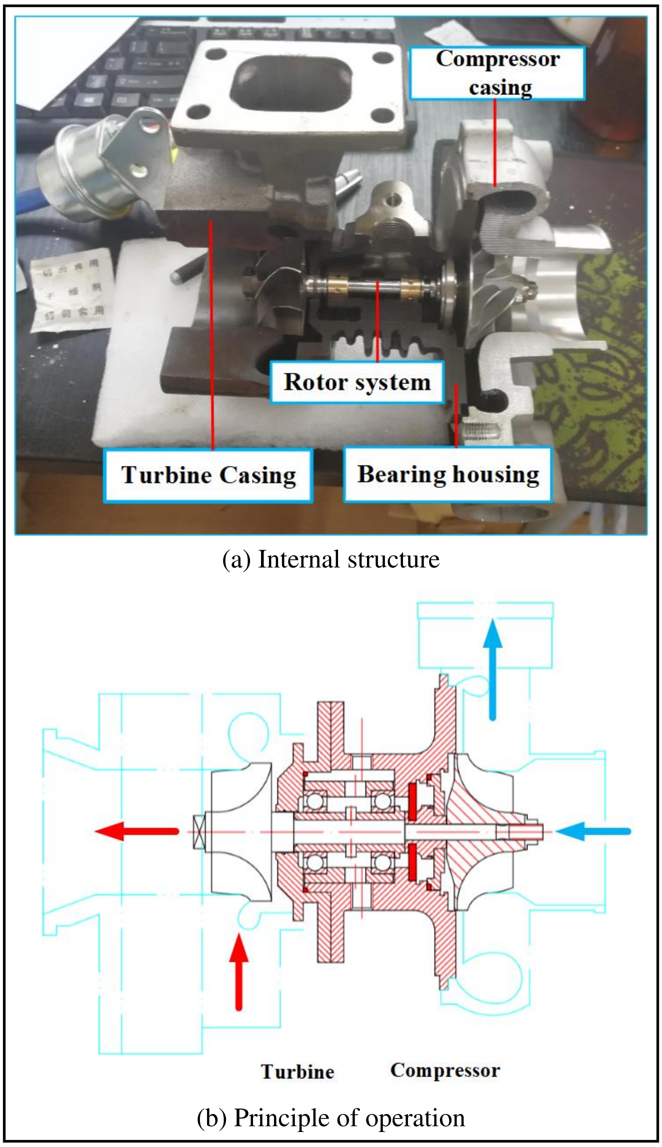

Figure 1. Structure of the micro-turbine.

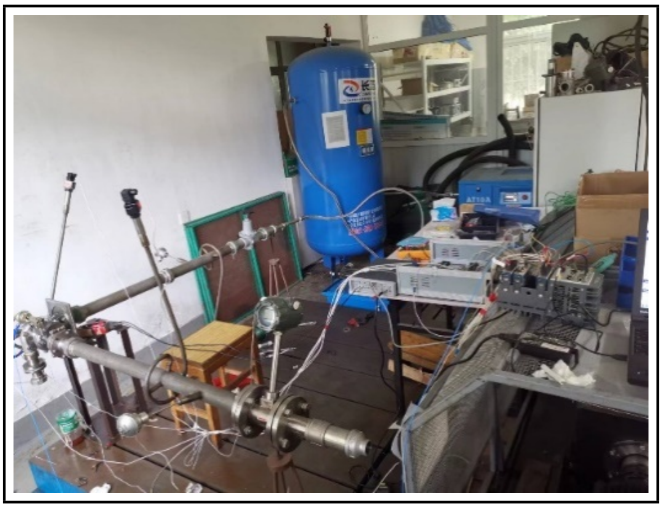

Figure 2. Airflow-driven micro-turbine experiment system.

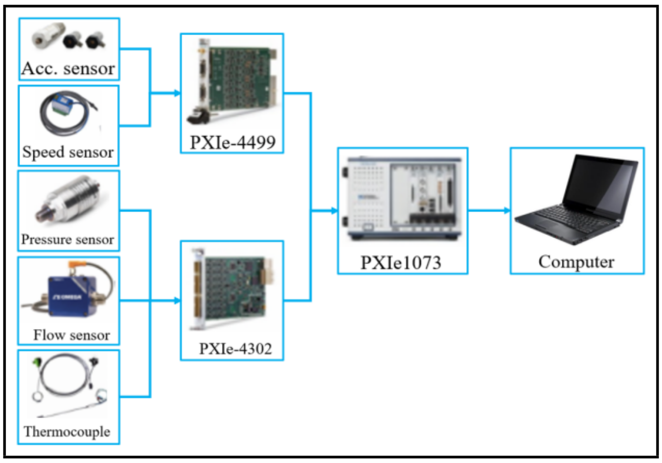

Figure 3. Measurement system for micro-turbine.

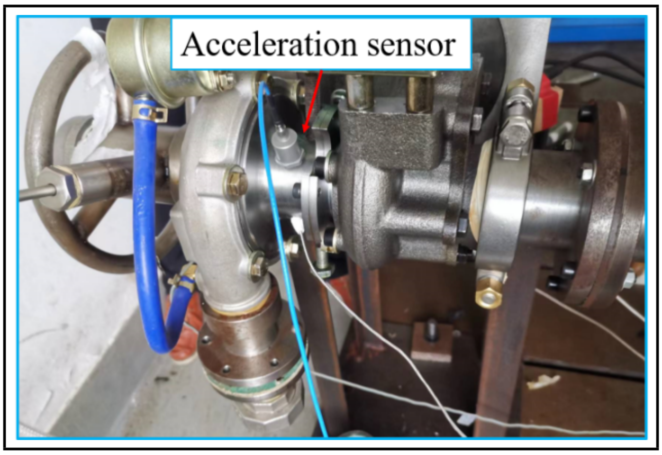

Figure 4. Acceleration sensor arrangement.

ply until stop, the approximate working time is no more than 30 seconds. In the experiment, several stable and unstable inlet flow cases were discovered by adjusting the valve openings of the inlet flow pressure repeatedly.

2.2. Measurement System

The measurement system is composed of an acceleration sensor, speed sensor, pressure sensor, flow sensor, thermocouple, NI data acquisition system and a computer as shown in Fig. 3.

The acceleration sensors arranged on the micro-turbine was shown in Fig. 4. The rotational speed sensor as shown in Fig. 5. The sampling frequency of speed signal and acceleration signal is 10240 Hz.

When the storage pressure is from 0.11 MPa–0.07 MPa, the micro-turbine outlet is opened only, and the time domain voltage signal plot is obtained as shown in Fig. 6(a). From the voltage time domain signal graph of the measured speed sensor in Fig. 6(a), it can be seen that when the probe of the speed sensor is relative to the flat part of the structural member, the voltage value is close to 0 V due to the far contact distance, when the circular arc part is relative to the front end of the probe, there is a voltage signal output with a voltage value of about 6 V, every two rectangular waves represent the impeller has rotated one revolution. After the calculation and signal extraction, it is transformed into the time domain curve of rotational speed as shown in Fig. 6(b).

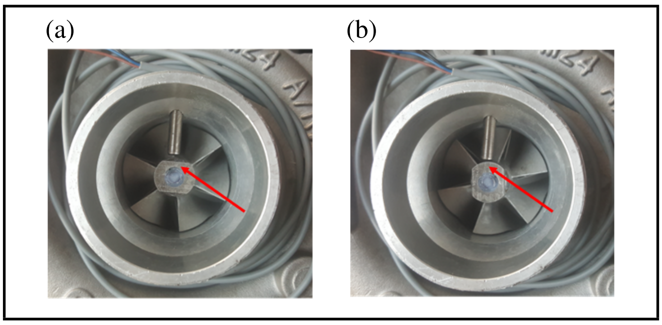

Figure 5. Operation of speed sensors for measuring rotational speed. (a) No output of voltage signal. (b) The output of a voltage signal.

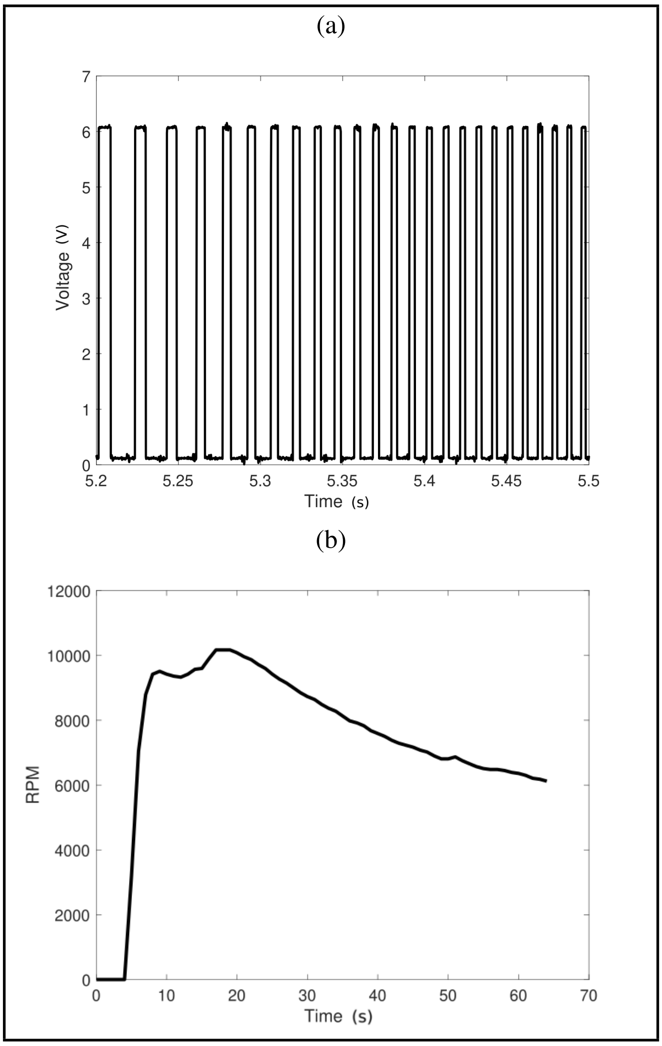

Figure 6. Measured speed data of Micro-turbine. (a) Voltage signal of the speed sensor. (b) Rotationgal speed in time domain.

2.3. Operating Cases in Experiment and Vibration Signal Analysis Methods

In this paper, by adjusting the opening and closing of inlet and outlet valves, unstable airflow is produced artificially, and the four groups of typical micro-turbine rotate speed conditions under different in-flows cases as shown in the Fig. 7.

According to the Fig. 7, it can be seen that each working condition has a relatively stable rotate speed fluctuation operating range. Therefore, the maximum and minimum values of the speed in each operating range are extracted, and the speed fluctuation rate is calculated. The calculation results are shown

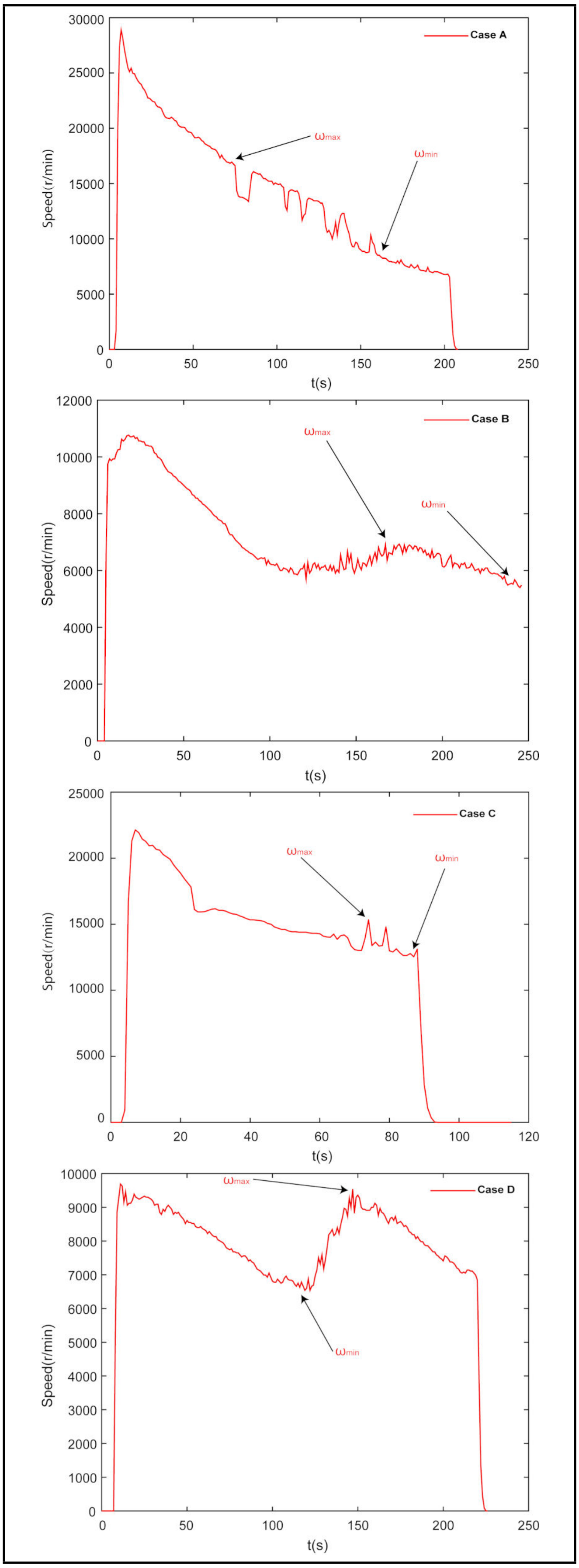

Figure 7. Measured speed data of Micro-turbine under 4 cases.

Table 1. Operating cases of stable and unstable inlet flows.

Case	Coefficient of speed fluctuation	Rotational speed (r/min)
A	33.33%	8000–16000
B	11.11%	6000–7500
C	10.34%	13000–16000
D	16.56%	6800–9500

in Table 1 and combined with the acceleration signal in this range for comprehensive analysis.

$$\delta_\omega = \frac{\omega_{max} - \omega_{min}}{\omega_{max} + \omega_{min}} \times 100\%; \tag{1}$$

where, δ_ω is coefficient of speed fluctuation, ω_{max} is max value of rotate speed in the process of working, ω_{min} is min value of rotate speed in the process of working.

The four selected speed conditions can cover the maximum speed measured in the experiment of about 30,000 r/min (condition A) and the minimum speed of about 10,000 r/min (condition D). And, for local fluctuation characteristics, there are also higher frequency repeated fluctuation conditions (condition B) and less fluctuation conditions (condition C). Four working conditions can be used to analyze the changes qualitatively and quantitatively in the speed values and bearing vibration signals caused by speed fluctuations of micro- turbine.

3. TIME AND FREQUENCY DOMAIN ANALYSIS

Time and frequency domain analysis includes time domain characteristic parameters (peak-to-peak value, RMS value and kurtosis value), statistical parameters (auto-correlation and BDS), and an amplitude spectra in frequency domains, as well as statistic spectrum indicators (SSI) based on Welch's periodogram of power spectra.

3.1. Time Domain Analysis

The measured vibration data were analyzed in time domains to obtain the waveform characteristics under different inlet flow conditions. Of the vibration signals, 0.05 seconds was extracted for analysis. The waveform of measured vibration signals on the micro-turbine under 4 cases is shown in Fig. 8.

The measured vibration signals are analyzed based on time domain methods. The formula of peak-to-peak, RMS, kurtosis values of vibration signals are as follows, and the waveform of these characteristic parameters are shown in Fig. 9.

$$X_{T_{pp}} = X_{T_{max}} - X_{T_{min}}; \tag{2}$$

$$X_{RMS} = \sqrt{\frac{1}{n} \cdot \sum_{i=1}^{n} x_i^2}; \tag{3}$$

$$X_{Kurtosis} = \frac{E(X-\mu)^4}{\sigma^4}; \tag{4}$$

where, μ is the mean of x, σ is the standard deviation of x, and $E(t)$ represents the expected value of the quantity t.

As shown in Fig. 9(a), there are significant differences in peak-to-peak values of vibration signals of the micro-turbines in the four cases. The peak-to-peak values of vibration signals in Case A are the highest, which are 2–4 times as high as those

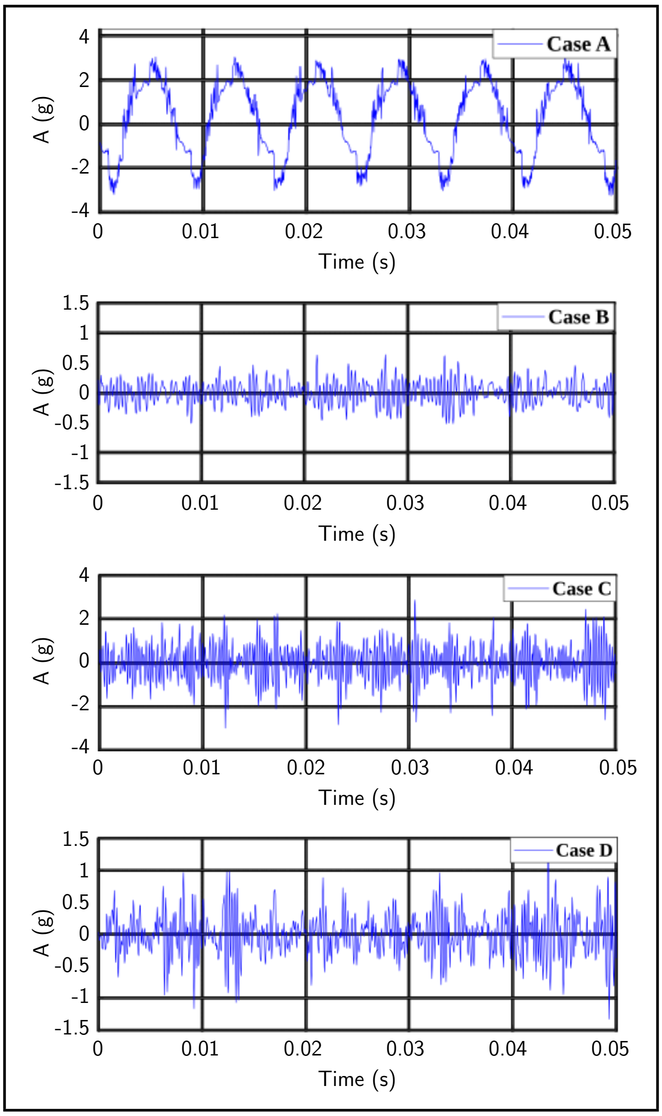

Figure 8. Waveform of measured acceleration signals on the micro-turbine under 4 cases.

in the other three cases. Meanwhile, the distinction between the other three cases is obvious, and the peak-to-peak values of Case B is the lowest. As shown in Fig. 9(b), there are also significant differences in the RMS values of vibration signals of micro-turbines in the 4 cases, among which the RMS values of Case A in the stable case are the highest, which are 4–6 multiple the RMS values of the other three cases. Meanwhile, the RMS values of the other three cases have little difference.

As shown in Fig. 9(c), there are certain differences in the kurtosis values of micro-turbine vibration signals under the 4 cases, among which the kurtosis values of Case D under the stable case are the highest, which is 2–3 times that of the kurtosis values in the other three cases. In addition, the kurtosis value is the lowest in Case A, and the curve of the kurtosis values that change with time are stable.

3.2. Statistical Analysis

3.2.1. Auto-correlation

Through the auto-correlation analysis of turbine vibration data, the periodic characteristics are found under four cases.

The auto-correlation of a signal is the dependency relationship between the instantaneous value of a signal at one mo-

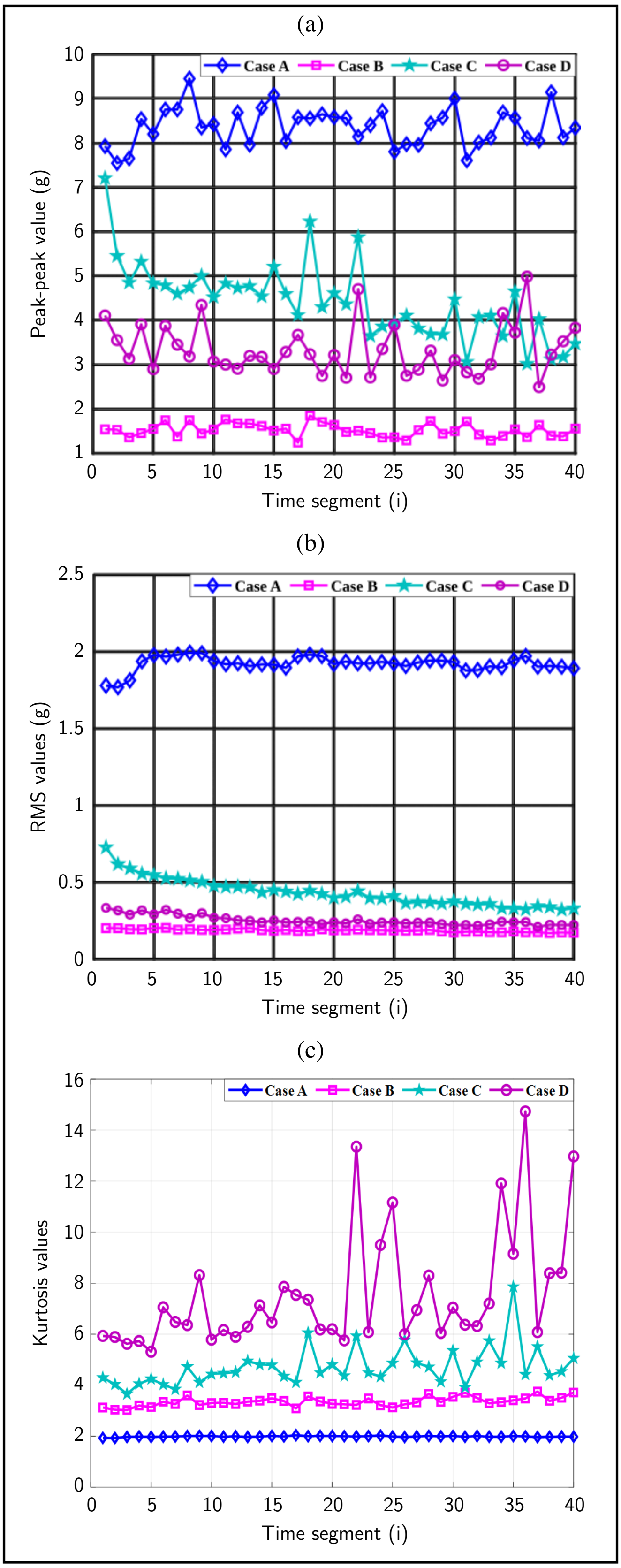

Figure 9. Numerical comparison of time domain characteristic parameters of micro-turbine vibration signals.(a) Comparison diagram of peak-to-peak values under 4 cases. (b) Comparison diagram of RMS values under 4 cases. (c) Comparison diagram of kurtosis values under 4 working cases.

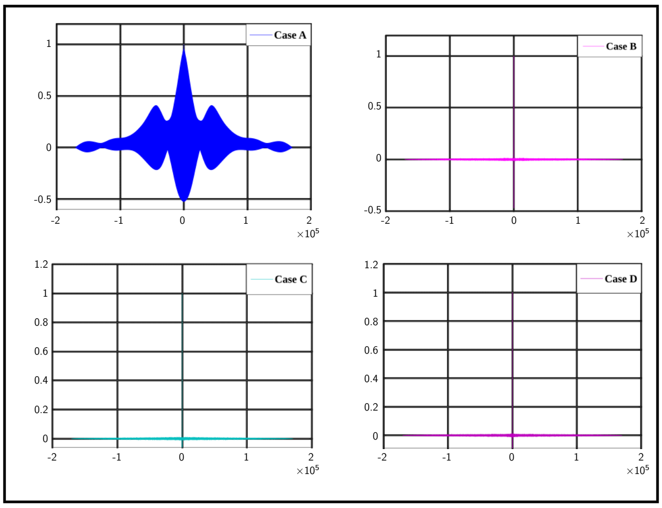

Figure 10. Auto-correlation values of measured vibration responses on the micro-turbine under 4 cases.

ment and the instantaneous value at another moment. Serial correlation, also called auto-correlation, refers to a time series $[X_t] = [\cdots, X_{-2}, X_{-1}, X_0, X_1, X_2, X_3, \cdots]$ these values are related to themselves before and after.

$$R(k) = \frac{E[(X_i - \mu_i)(X_{i+k})]}{\sigma^2}. \tag{5}$$

Comparing these two formulas, it can be seen that auto-correlation is the change in the correlation coefficient between $[X_t]$ and $[X_{t+k}]$, which changes from two random variables to one random variable. The auto-correlation values of measured vibration responses on the micro-turbine under four cases are shown in Fig. 10.

As shown in Fig. 10, where the noise in Case A has a wide and uniform spectrum of random signals. Regular and periodic pulses appear in the vibration signal in the case of unstable inlet flow.

3.2.2. BDS test

BDS test is used to analyze non-linearity in the time series measured micro-turbine vibration signals.

The BDS test is a non-parametric test for serial independence based on the correlation integral of the scalar series, $[x_t]$. For embedding dimension m, let $[x_t^m]$ denote the sequence of m-histories generated by $[x_t]$:

$$[x_t^m] = [x_t,\ x_{t+1},\ \cdots,\ x_{t+m-1}]. \tag{6}$$

Then the correlation integral $C_{m,T}(\varepsilon)$ for a realization of T is given by:

$$C_{m,T}(\varepsilon) = \sum_{t<s} I_\varepsilon(x_t^m, x_s^m) \left\{ \frac{2}{T_m(T_m - 1)} \right\}; \tag{7}$$

where, $T_m = T - (m-1)$ and $I_\varepsilon(x_t^m, x_s^m)$ is an indicator function which equals one if the sup norm $\|x_t^m - x_s^m\| < \varepsilon$ and equals 0 otherwise. The asymptotic normality $C_{m,T}(\varepsilon)$ under the null hypothesis that $[x_t]$ is known as an independent identical distribution process to obtain a test statistic that asymptotically converges to a unit normal.

The BDS test values of the vibration signals of Case A, B, C, and D of measured vibration responses on the micro-turbine casing under 4 cases as shown in Fig. 11.

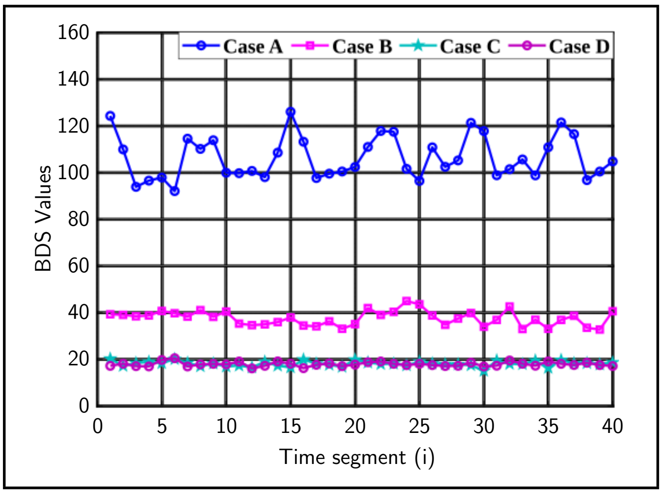

Figure 11. BDS values of measured vibration responses on the micro-turbine under 4 cases.

As shown in Fig. 11, it can be found that the BDS values of Case A are much larger than the three others. But there is no great difference between Case C and Case D.

3.3. Amplitude Spectra

The distribution of signal amplitude with frequency is analyzed by Fourier amplitude spectrum analysis of measured vibration data.

$S(f)$ is FFT result of signal $s(t)$:

$$S(f) = \int_{-\infty}^{\infty} s(t)e^{-j2\pi ft}dt. \tag{8}$$

The amplitude spectra based on vibration signals FFT of a micro-turbine in stable and unstable cases at different rotational speeds are calculated. In the frequency domain description of a signal, the frequency is used as the independent variable, and the amplitude of each frequency component of the signal is used as the dependent variable. This is called the amplitude spectrum. The amplitude spectra of measured vibration responses on the micro-turbine casing under 4 cases are shown in Fig. 12.

As shown in Fig. 12, the amplitude spectrum was performed for all 4 cases. There are still great differences as it has been found that the vibration signal of Case B, C, and D has meaningless peaks in the high-frequency region and the vibration amplitude is not large.

4. POWER SPECTRA AND STATISTIC SPECTRUM ANALYSIS

4.1. Waterfall of Power Spectra

The waterfall diagram is used to analyze these disproportionate instantaneous spectra. It is very beneficial to highlight the characteristics that change with speed. It uses the method of short-time FFT transform to calculate the instantaneous power spectrum and display the analysis results. The power spectrum method is to analyze the signal with limited power vibration signals, which shows the change of signal power with frequency.

$P(f)$is power spectral density (PSD) of signal $s(t)$:

$$P(f) = \lim_{T\to\infty} \frac{1}{T}|S(f)|^2; \tag{9}$$

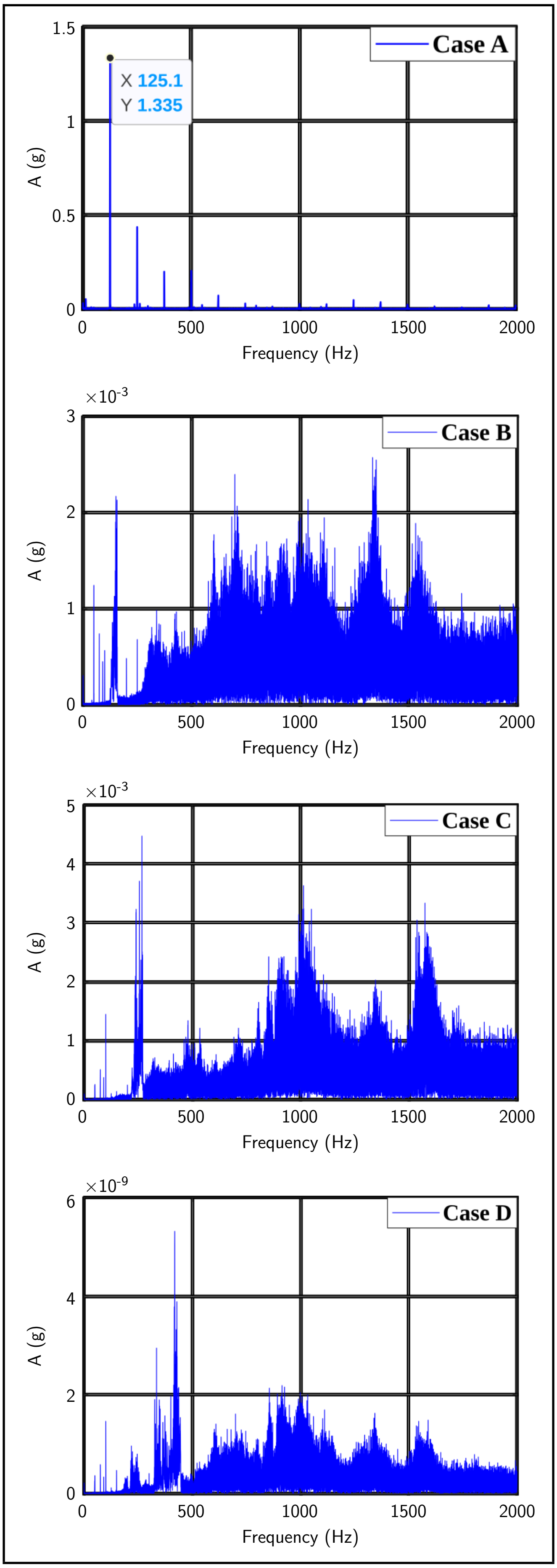

Figure 12. Amplitude spectra of measured vibration responses on the micro-turbine casing under 4 cases.

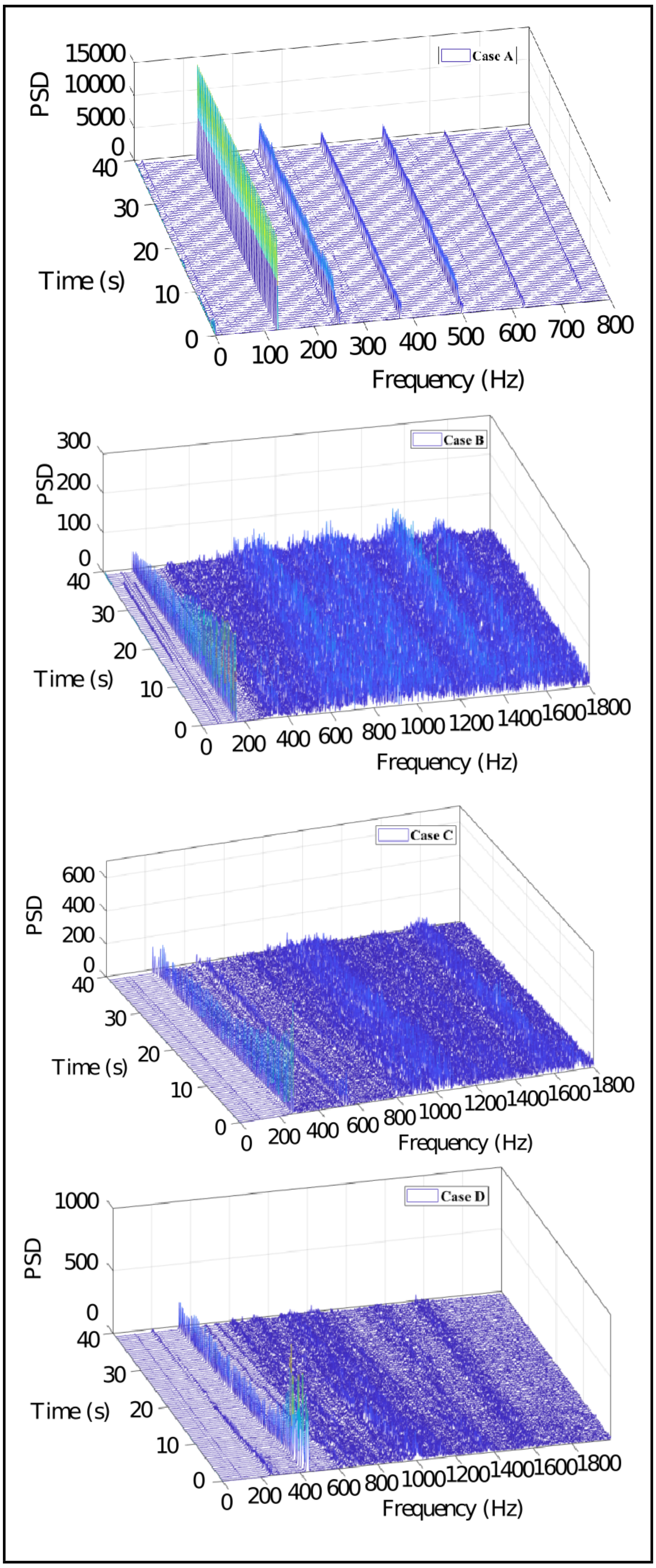

Figure 13. Waterfall diagram of measured vibration responses on the micro-turbine casing under 4 cases.

where $S(f)$ is FFT result of signal $s(t)$ referring to Eq. (8).

The waterfall diagram of measured vibration responses on the micro-turbine casing under 4 cases as shown in Fig. 13.

As shown in Fig. 13, the diversity of the micro-turbine vibration signal amplitude under stable and unstable case is obvious, and the rotational speeds factually affect the micro-turbine vibration signal.

4.2. Statistic Spectrum Analysis

The statistic spectrum indicator (SSI) method is introduced to statistically analyze the power spectrum of the signal.

The SSI method is based on Welch's periodogram of power spectra. The processing technique is as follows, the average of the power spectra is computed on subsegments of the vibration responses, where Welch's method adds overlapping between the different subsegments and windowing of the subsegments in order to reduce the side effect. Then, let $x(n)$ be a signal of length N and $w(n)$ be a window function. Considering subsegments of length L with 50% overlap, Welch periodogram P_w is the average of the periodogram P_i computed on the $K = N/(2L+1)$ sub-segments and expressed as:

$$P_W = \frac{1}{K}\sum_{i=0}^{K-1} P_i; \tag{10}$$

with P_i being the periodogram computed on the i-th subsegment as:

$$P_i = \frac{|\sum_{n=0}^{L-1} w(n)x(n+i\frac{L}{2})e^{-jn\omega}|^2}{\sum_{n=0}^{L-1}|w(n)|^2}. \tag{11}$$

The advantage of this method is to reduce power spectrum variance. The next step is the statistical processing of the periodogram P_w in order to center and to reduce it. The spectral power in dB at the frequency f_i, is considered to be a random variable following a normal distribution over the recordings and noted $P_w(f_i) = 20\log(P_w(f_i))$. The statistic-based indicator S is computed in the following way, for each recording r, the Welch's periodogram $P_w(f)$ of the stator current is computed. The first n_{ref} periodogram are stored to compute the reference averages and standard deviations for each frequency. Once the reference has been built, the next periodogram are centered and reduced.

When comparing the SSI of measured micro-turbine's vibration responses under stable cases, the unstable case in lower and higher rotating speeds results in the SSI values of the 4 cases as shown in Fig. 14.

As shown in Fig. 14, the shapes of the curves differ for several cases, and the SSI values for the different cases can be clearly separated. The SSI values for Case A with stable inflow under 9000 r/min, are significantly higher than the other three cases with unstable inlet flow.

5. TIME-FREQUENCY DOMAIN ANALYSIS

5.1. Hilbert-Huang Transform

The HHT method is a time-frequency adaptive signal processing method after the Fourier transform and wavelet transform. The HHT mainly includes two main parts: empirical mode decomposition (EMD) and Hilbert spectral analysis. The signal $x(t)$ can be divided into the number of n intrinsic mode functions (IMF) by EMD.

$$x(t) = \sum_{j=1}^{n} c_j(t) + r_n(t); \tag{12}$$

then apply the Hilbert transform to all IMFs.

$$H[c_j(t)] = \frac{1}{\pi}\int_{-\infty}^{\infty}\frac{c_j(\tau)}{t-\tau}\mathrm{d}\tau. \tag{13}$$

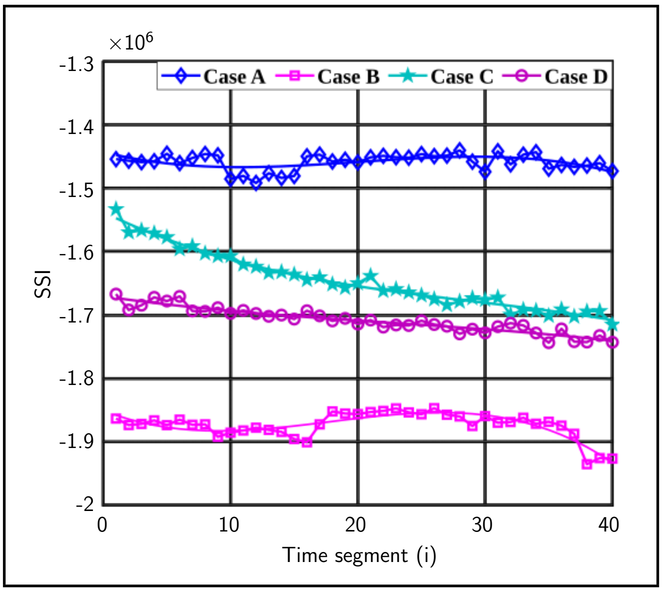

Figure 14. SSI values of measured vibration responses on the micro-turbine under 4 cases.

Therefore, the Hilbert spectrum $H(\omega, t)$, shown in the following equation, is a time-frequency energy spectrum, which both the frequency variation at different time periods and the energy variation with time and frequency can be seen.

$$H(\omega, t) = \text{Re}\left(\sum_{i=1}^{n} a_i(t)e^{j\int \omega(t)\text{d}t}\right). \tag{14}$$

The marginal spectrum $h(\omega)$ as follows:

$$h(\omega) = \int_0^T H(\omega, t)\text{d}t; \tag{15}$$

The 1st seconds data of the four groups of measured micro-turbine's vibration responses are decomposed by the EMD, and the spectrum of IMF components with different orders is calculated, as shown in Fig. 15–18. By comparison, it can be found that these IMF components are different and have a certain pattern of variation. The calculated HHT marginal spectra of the above four cases of vibration signals are shown in Fig. 19.

As shown in Fig. 15, broadband random characteristics of order 1–6th, energy is not uniform along the frequency band, or symmetrical distribution with a frequency as the midpoint.

As shown in Fig. 16, the orders 1–4th are narrow-band random distributions with 2909, 1681, 905, and 581 Hz as the center frequency and relatively concentrated energy distribution. The 11th order above, which mainly belong to VLF and DC components, can be omitted. The orders 5-6th order are 2-fold,1-fold, half-fold, 1/3-fold and their combinations with certain random components and the 6th order has a unique and prominent trans-conversion component.

As shown in Fig. 17, the order 1–4th is a narrow-band random distribution with 3863, 2637, 1055, 807 Hz as the center frequency and relatively concentrated energy. The 5th order is the rotational frequency, which is very prominent; the 6th order is 1 time and 2 times the rotational frequency and it combines with a certain random component.

As shown in Fig. 18, the 1st–4th order is a narrow-band random distribution with 4210, 2890, 1009, 807, 500 Hz as the center frequency and relatively concentrated energy. The 5th-6th orders are the eigenfrequencies of 1 and 1/2 times the trans-conversion frequency with some random components.

As shown in Fig. 19, the comparison of the marginal spectrums of Case A and B can clearly show the components close to the rotational frequency, but the marginal spectrum of Case B has two components of 784 Hz and 3024 Hz with the amplitude about 1/3 of the amplitude of the rotational frequency component, which means that Case A is a relatively stable vibration.

The marginal spectrum of Case C clearly shows the components close to the transient frequency, in addition to the component of 4144 Hz, the amplitude is about 3/5 of the transient frequency component amplitude. The marginal spectrum of Case D clearly shows the components close to the transient frequency, in addition to the components at 3000 Hz and 4500 Hz, which are about 1/6 of the transient frequency component amplitude.

5.2. Phase Spectra

The phase spectra based on the Hilbert transform (HT) of the micro-turbine vibration signals is to compare different inlet flow cases.

The analytic signal is obtained by a HT of the line current spectrum modulus. When considering signal $s(t)$, the analytic signal $\tilde{s}(t)$ can be expressed as:

$$\tilde{s}(t) = s(t) + j\rho(t). \tag{16}$$

The $\rho(t)$ represents the HT of the signal $s(t)$ is given by the following equation:

$$\rho(t) \xrightarrow{HT} -j\text{sgn}(\omega)S(f); \tag{17}$$

where $S(f)$ is the Fourier Transform of $S(t)$, and $\text{sgn}(\omega) = [1, 0, -1]$, when $\omega > 0$, $= 0$ < 0.

Consequently, the analytic signal phase $\Psi_{HT}(\omega)$ can be calculated with the expression:

$$\Psi_{HT}(\omega) = \arctan\frac{\text{Im}(\tilde{Y}(\omega))}{\text{Re}(\tilde{Y}(\omega))} = \arctan\frac{Y_{HT}(\omega)}{|Y(\omega)|}. \tag{18}$$

The phase spectra of measured vibration responses on the micro-turbine casing under 4 cases as shown in Fig. 20.

As shown in Fig. 20, with the same speed of 9000 r/min, the vibration signal phase of the micro-turbine with the stable and unstable inlet flow case changed greatly. The phase diagram for the unstable inlet flow case under different rotational speeds have similar graphs, but all of them are significantly different from the stable case.

6. NONLINEAR FEATURE ANALYSIS

The vibration signals of unsteady inlet flow are characteristics for nonlinear, and the vibration responses of four working conditions are compared and analyzed by several nonlinear feature analysis methods.

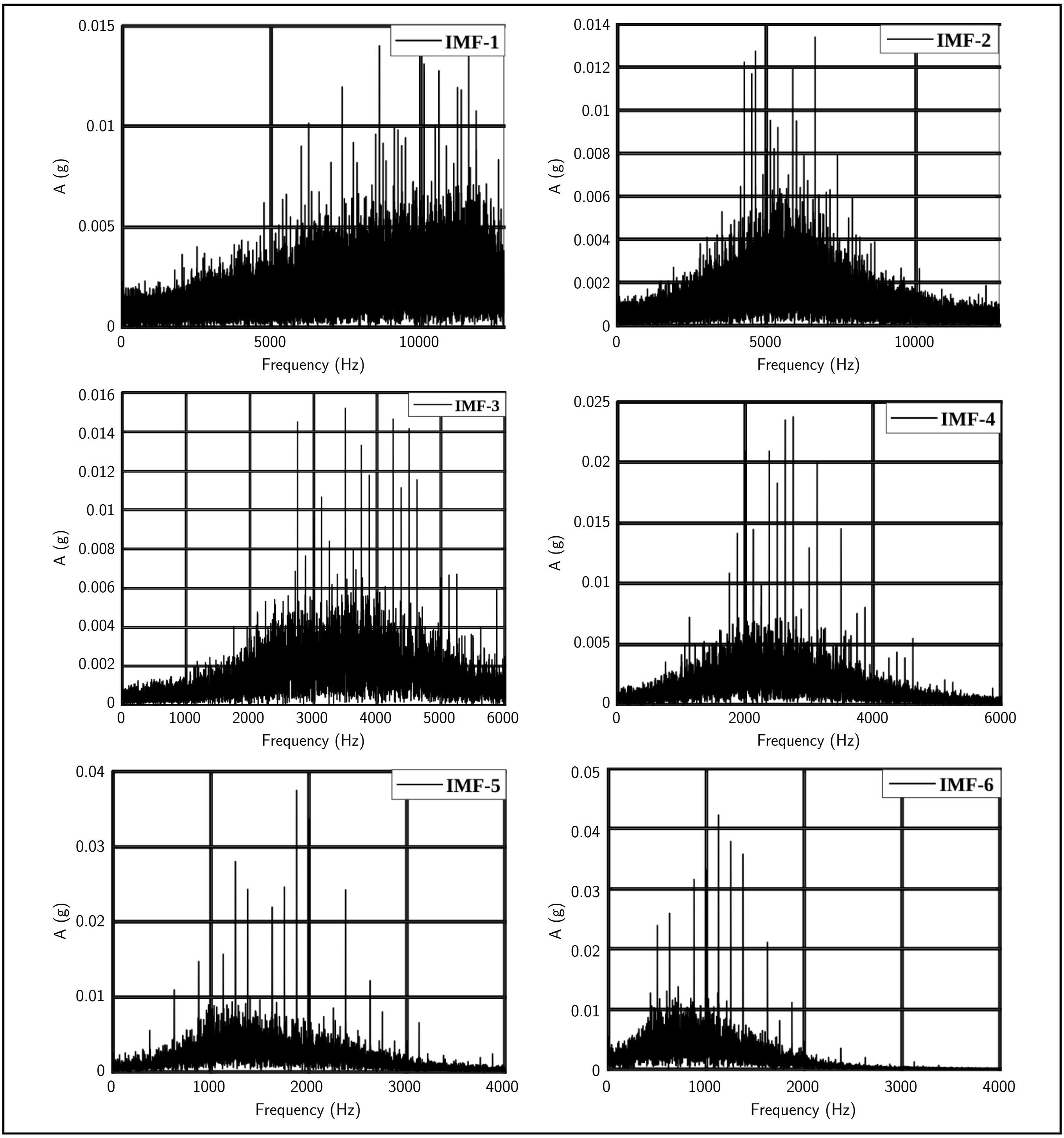

Figure 15. The spectrums of the IMF of Case A by EMD.

6.1. Phase Space Reconstruction

The phase space reconstruction is an effective method to excavate the deep level information of the nonlinear time series, such as micro-turbine vibration signals.

The phase space reconstruction is the recovery of the original system from a time series based on the Takens delay embedding theorem. It reconstructs an equivalent state space as a common method. Only one component is examined and its measurement at some fixed point of time delay is used as the new dimension, which preserves many properties of the original system. Therefore, the comparison of micro-turbine vibrations under stable and unstable inlet flow cases based on phase space reconstruction can distinguish the different behaviors of the vibrations, as shown in Fig. 21.

As shown in Fig. 21. It can be observed that the Pseudo-Poincare mapping diagrams under different cases can be valued separability and are consistent within themselves. The Pseudo-Poincare mapping diagrams of the Case A is obviously different from the other cases of unstable inlet flow, with a large difference and distinction, and has obvious attractor characteristics. The distribution range of the Pseudo-Poincare mapping diagrams under high rotating speeds is relatively concentrated, with the characteristics of random signal.

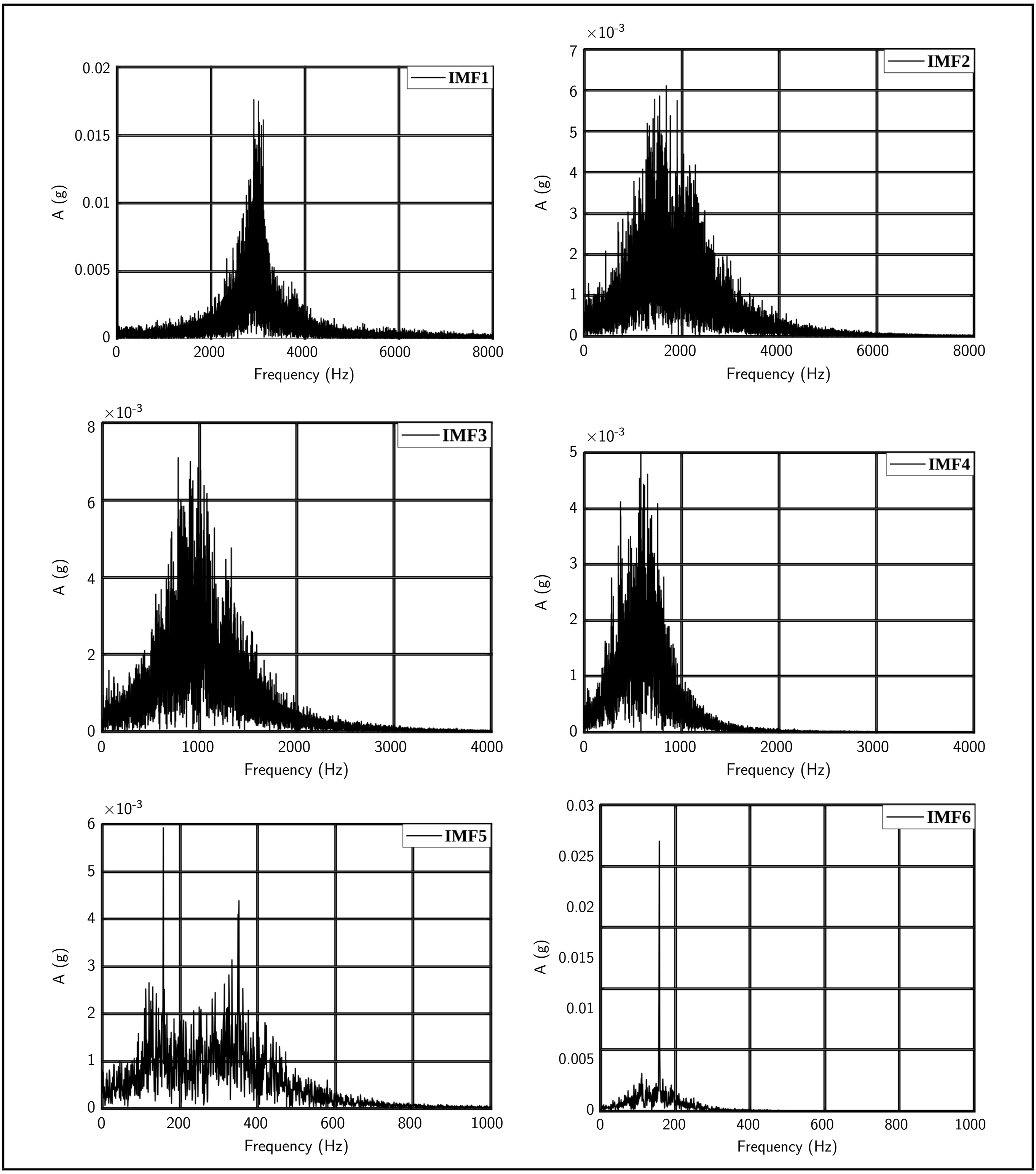

Figure 16. The spectrums of the IMF of Case B by EMD.

6.2. Lempel-Ziv Complexity

The LZ complexity values, reflect the rate of generating new patterns as the length of the measured micro-turbine vibration signals sequence grows.

It can describe the process of sequence changes, and a characteristic parameter for the state of the system represented by the signal. The complexity has been widely used as an important nonlinear indicator in time series analysis. The algorithm for the LZ complexity is as follows:

1) Reconfiguration sequence, $\{x_1, x_2, \dots, x_n\}$ if:

$$S_i = \begin{cases} 1, & x_i \geq \bar{x} \\ 0, & x_i < \bar{x} \end{cases}; \tag{19}$$

what, $\bar{x} = ()x_1, x_2, \dots, x_n)/n$.

2) $S = (s_1, s_2, \dots, s_r)$, $r < n$, $Q = s_{r+1}$.

3) Repeat the above steps for all characters before ”O”.

4) The number of $C(n)$ segments into which the string is ”O” divided is the complexity of the sequence, obviously $C(4) = 3$.

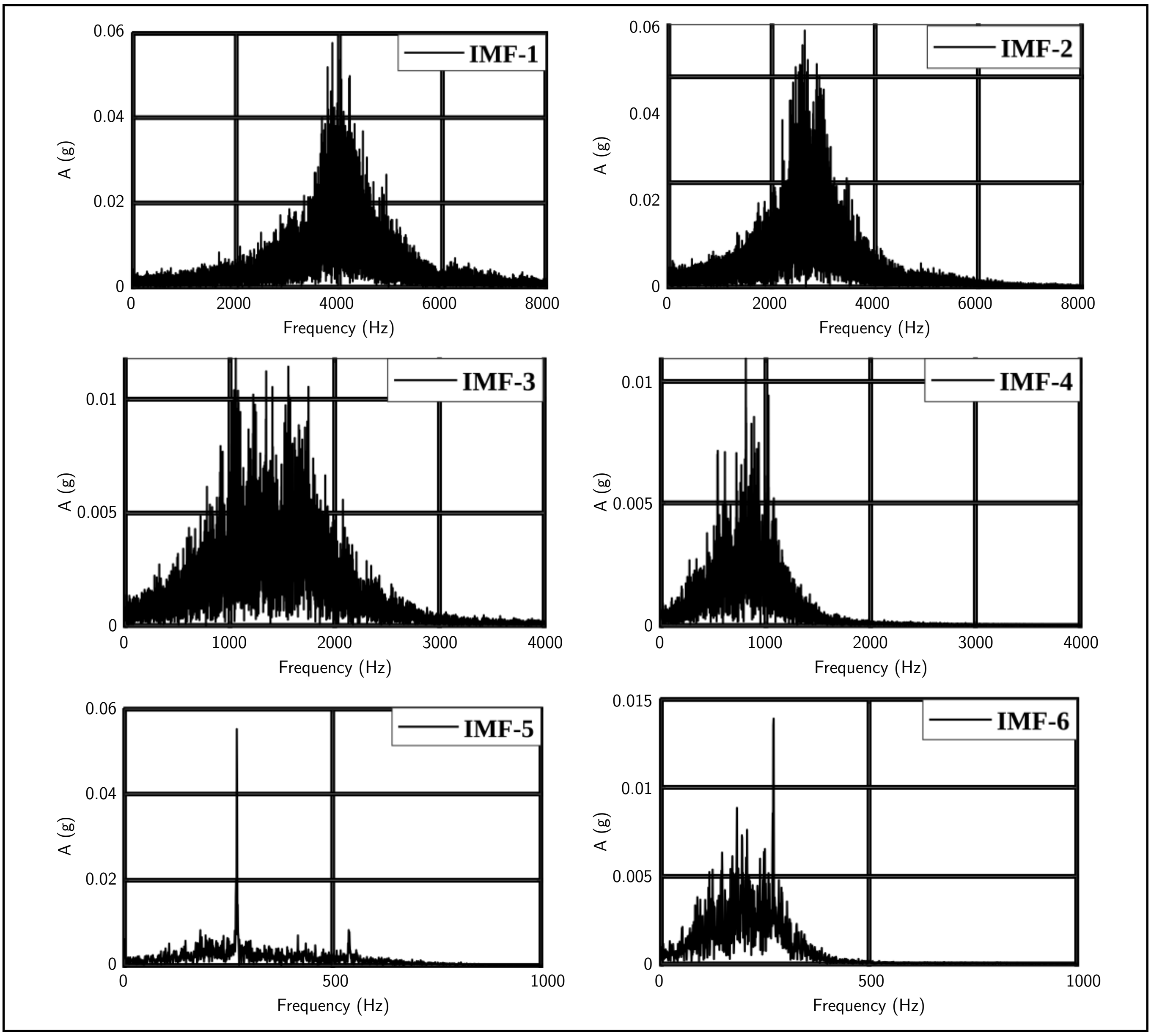

Figure 17. The spectrums of the IMF of Case C by EMD.

5) The complexity of almost all 0, 1 random sequence tends to $B(n) = n/\log n$. The relative complexity $R(n) = C(n)/B(n)$, which reflects how close a sequence is to a random sequence, is obtained.

The LZ complexity values of the micro-turbine measured vibration signals are shown in Fig. 22.

From the Fig. 22, the following conclusions can be drawn: The LZ complexity values under different cases have separability and consistency. Therefore, there are comparable conditions when discussing the complexity. The complexity values for Case A with 9000 r/min stable airflow are significantly lower than the other three cases with unstable inlet flow. The value of complexity under high rotational speed cases is slightly higher than the value of low rotational speed with a regular process.

7. CONCLUSION

In this article, the vibration behavior of the micro-turbine under stable and unstable inlet flows under different rotational speeds is quantitatively characterized in time domain, statistical parameters frequency domain, SSI, time-frequency domain, and nonlinear feature analyzing methods, which provides a theoretical reference for the aerodynamic stability monitoring of the environmentally controlled micro-turbine system and the improvement of the environment controlled micro-turbine design. The main conclusions are as follows:

(1) The paper provided a detailed comparative analysis of the vibration behavior characteristics of the airflow-driven micro-turbine system. This provided a theoretical support and data analysis based on bearing vibration signals can effectively characterize the operation status of micro-turbine under severe conditions such as rapid and frequent speed changes. The characteristic parameters of time-domain analysis, such as peak to peak and RMS can clearly characterize the difference between relatively stable and relatively unstable intake, while the kurtosis value is not obvious. Autocorrelation analysis has a poor performance in characterizing working conditions with similar rotational speeds.

(2) From the perspective of spectrum analysis methods, the

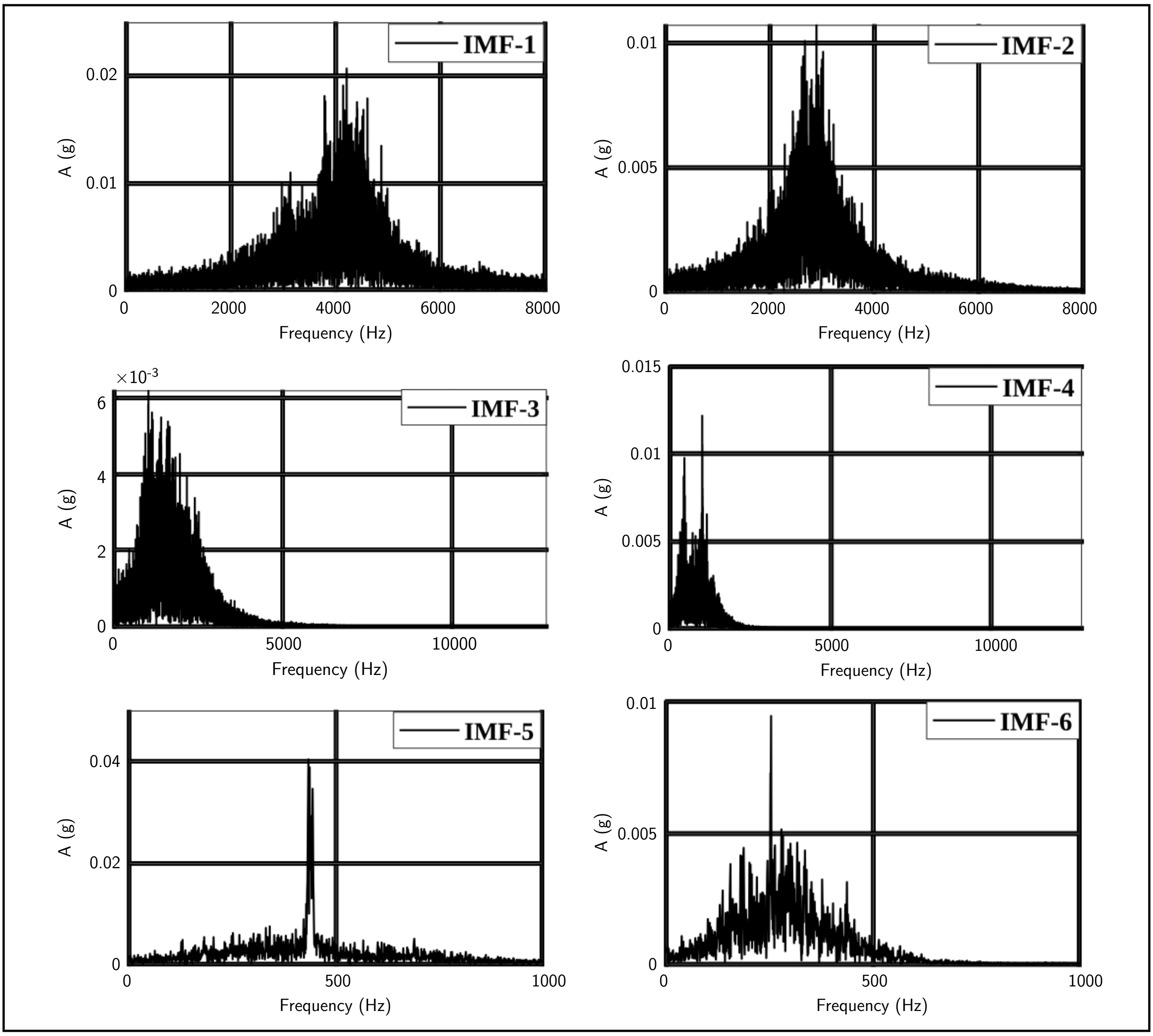

Figure 18. The spectrums of the IMF of Case D by EMD.

higher frequency component energy was weaker under micro-turbine high speed unstable conditions, while the lower frequency component energy was weaker under low speed stable conditions. SSI analysis effectively characterized the frequent changes in intake and relatively stable intake conditions of micro turbines. BDS values were ideal for characterizing conditions with large speed differences, such as operating conditions A and D with amplitudes that differ by up to 4 times. However, both of BDS values and HHT spectrum analysis have weaker effects under operating conditions with similar speeds.

(3) The nonlinear analysis methods had good performances in characterizing both rapid and frequent variable speed operating conditions of the micro-turbine, especially when the LZ complexity was used to quantitatively evaluate the operating status of micro- turbine. The amplitude difference between operating conditions A and D was up to 2 times.

(4) First, efforts should be made to avoid the large amplitude and rapid speed operating conditions of micro-turbines, which can cause a sharp increase in the acceleration of bearings and rotating shafts. If it is accompanied by poor lubrication and other conditions, it is highly likely to lead to premature failure and serious accidents. For micro turbines that often operate under large amplitude and small amplitude frequent variable speed conditions, the nonlinear analysis method based on vibration signals can be applied to different characteristic operating conditions, resulting in advantages of strong adaptability and good characterization effect.

ACKNOWLEDGMENTS

This research work was supported by the National Key R&D Program of China (No. 2020YFB2006800).

REFERENCES

[1] Feng, Y., Wang, J. D., Han, D. J. Experimental study on rotor vibration characteristics of high speeds micro-turbine generators. *Noise and Vibration Control*, 2019. **39**(14):95–100.

[2] Tian, Y., Zhong, Y., Liu, H., et al. Effects of turbulent

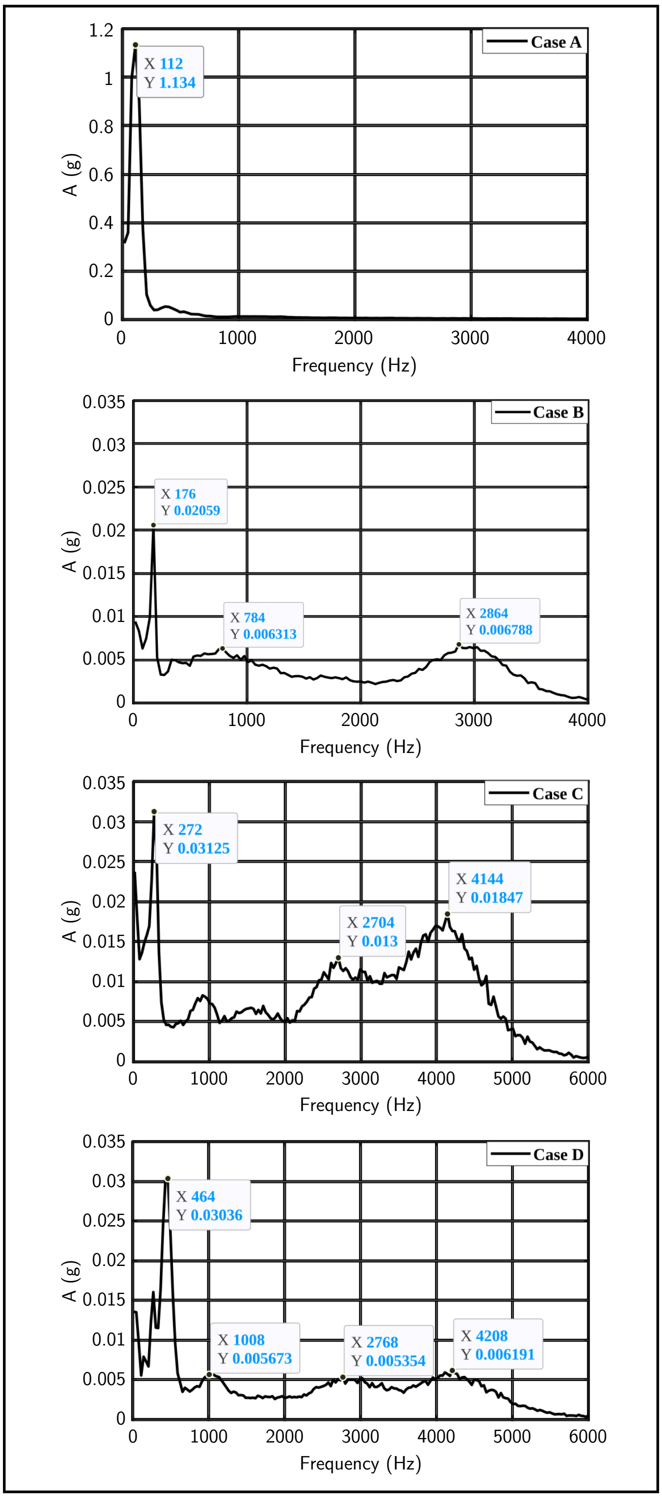

Figure 19. Marginal spectrums of measured vibration responses on the micro-turbine under 4 cases.

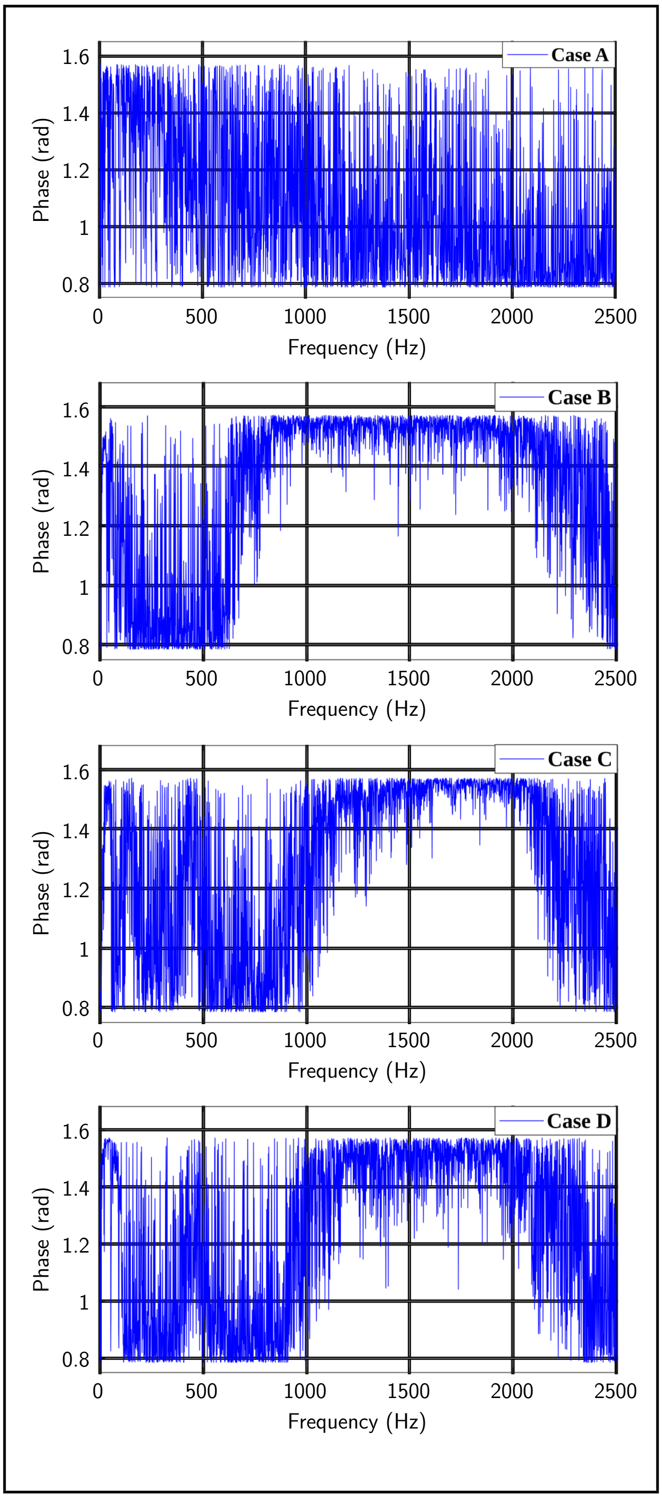

Figure 20. The phase spectra of measured vibration responses on the micro-turbine under 4 cases.

wind and irregular waves on the dynamic characteristics of a floating offshore wind turbine platform. *Journal of Mechanical Science and Technology*, 2023. **37**(6):2921–2931. https://doi.org/10.1007/s12206-023-0518-2

[3] Chun, Y. H., Ahn, J. Effects of geometric parameters of a staggered labyrinth seal on leakage flow. *Journal of Mechanical Science and Technology*, 2023, **37**(6):2959–2968. https://doi.org/10.1007/s12206-023-0522-6

[4] Wei, X., Yao, Z., Jin, F., et al. Numerical simulation of flow and heat transfer characteristic in straight-through labyrinth seals of aeroengines under eccentric and rotating conditions. *Journal of Mechanical Science and Technology*, 2023, **37**(6):3173–3183. https://doi.org/10.1007/s12206-023-0541-3

[5] Liu, X., Chen, G., Wei, X., et al. A rolling bearing fault evolution state indicator based on deep learning and its application. *Journal of Mechanical Science and Technology*, 2023, **37**(6):2755–2769. https://doi.org/10.1007/s12206-023-0504-8

[6] Fu, X., Li, D., Wang, H., et al. Analysis of transient flow in

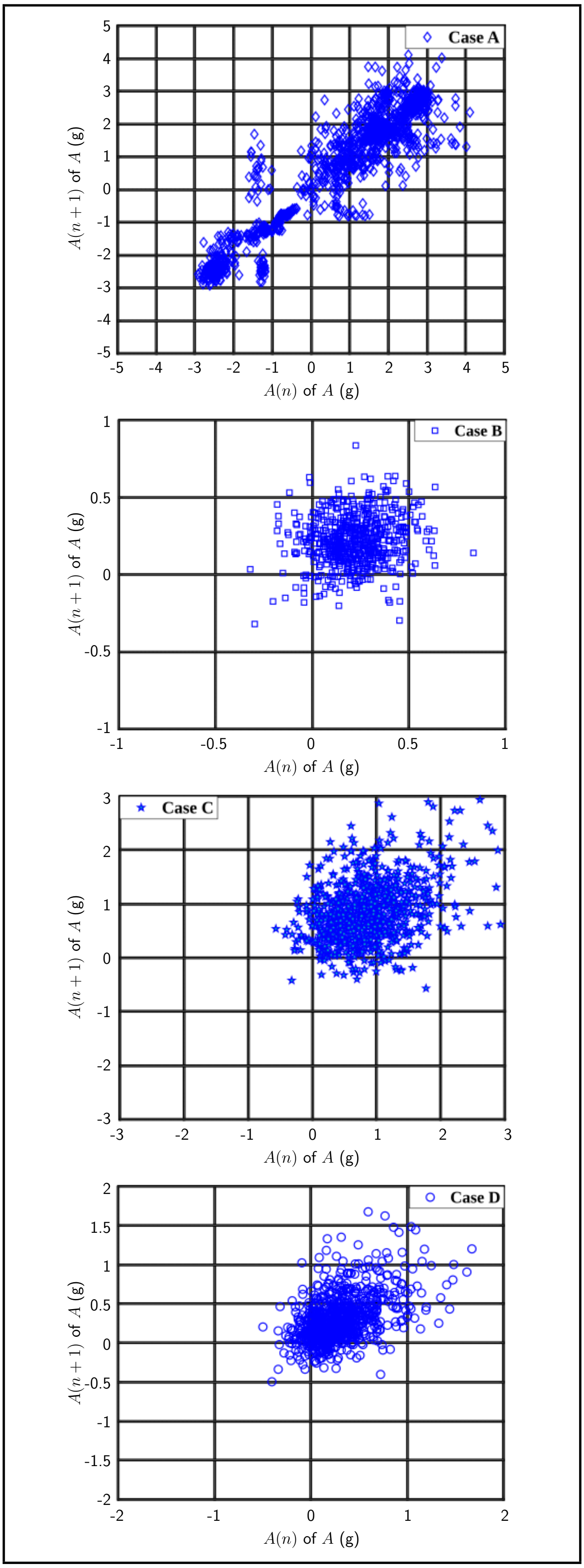

Figure 21. Pseudo-Poincare mapping diagrams of measured vibration responses on the micro-turbine under 4 cases.

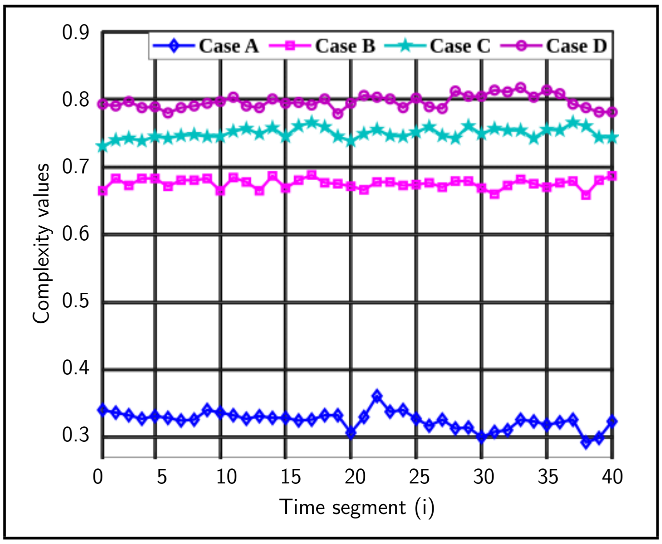

Figure 22. LZ complexity values of measured vibration responses on the micro-turbine under 4 cases.

a pump-turbine during the load rejection process. *Journal of Mechanical Science and Technology*, 2018, **32**(5):2069–2078. https://doi.org/10.1007/s12206-018-0416-1

[7] Yoon, J., Lee, M., Joo, S., et al. Instability mode and flame structure analysis of various fuel compositions in a model gas turbine combustor. *Journal of Mechanical Science and Technology*, 2015, **29**(3):899–907. https://doi.org/10.1007/s12206-015-0203-1

[8] Inoue, M., Kuroumaru, M., et al. Detection of a Rotating Stall Precursor in Isolated Axial Flow Compressor Rotors. *Journal of Turbomachinery*. 1991, **113**(2): 281–287. https://doi.org/10.1115/1.2929102

[9] Hendricks, G. J., Sabnis, J. S., and Feulner, M. R. Analysis of Instability Inception in High-Speed Multistage Axial-Flow Compressors. *Journal of Turbomachinery*. 1997, **119**(4):714–722. https://doi.org/10.1115/1.2841181

[10] Meng, F. X., Sun, J. N., et al. Modeling and validating of air cycle machine in aircraft environmental control system. *CIESC Journal* **71**(S1) (2020) 328–334.

[11] Song, J. X., Lin, G. P., et al. Transient performances of air-bleeding part of environmental control system. *Journal of Beijing University of Aeronautics Astronautics*, 1997. **23**(5) 560–564.

[12] Zhao, J. Q., Lin, G. P., et al. Experimental study of the dynamic responses of the ECS's bleed system. *Journal of Beijing University of Aeronautics Astronautics*. 2000, **26**(5):527–529.

[13] Gu, C. W., Yamaguchi, W., Nagashima, T. Research on the instability of centrifugal compressors. *Journal of power engineering*. 2006, **26**(2):196–200.

[14] Elasha, F., Shanbr, S., Li, X., and Mba, D. Prognosis of a wind micro-turbine gearbox bearing using supervised machine learning, *Sensors*, 2019. vol. **19**, no. 14, pp.3078–3092. https://doi.org/10.3390/s19143092

[15] Udmale, S. S., and Singh, S. K. Application of spectral kurtosis and improved extreme learning machine for bearing fault classification, *IEEE Transactions on Instrumentation and Measurement*, 2019. vol. **68**, no. 11, pp. 4222–4233. https://doi.org/10.1109/TIM.2018.2890329

[16] Jin, Z. H., Han, Q. C., Zhang, K., et al. An intelligent fault diagnosis method of rolling bearings based on Welch power spectrum transformation with radial basis function neural network. *Journal of Vibration and Control* 2020, Vol. **26**(9–10):629–642. https://doi.org/10.1177/1077546319889859

[17] Pei, D., Yue, J. H., Jiao, J. Weak fault feature extraction of rolling bearing based on autocorrelation and energy operator enhancements. *Journal of Vibration and Shock*, 2021, **40**(11):101–108+123. https://doi.org/10.13465/j.cnki.jvs.2021

[18] Brock, W. A., Dechert, W. D., Scheink-man, J.A. A test for independence based on correlation dimension. *Economic Review*. 1996, **15**(3):197–235. https://doi.org/10.1080/07474939608800353

[19] Picot, A., Obeid, Z., Régnier, J., et al. Statistic-based spectral indicator for bearing fault detection in permanent-magnet synchronous machines using the stator current, *Mechanical Systems and Signal Processing*, 2014, **46**(2):424-441. https://doi.org/10.1016/j.ymssp.2014.01.006

[20] Picot, A., Obeid, Z., Poignant, S. et al. Bearing fault detection in synchronous machine based on the statistical analysis of stator current, *Proceedings of the 38th Conference on IEEE Industrial Electronics Society*, IECON'12, Montreal, Canada, 2012. https://doi.org/10.1109/IECON.2012.6389275

[21] Chen, G., Chen, J., and Dong, G. Chirplet Wigner-Ville Distribution for Time-Frequency Representation and Its Application, *Mechanical Systems and Signal Processing*, 2013, **41**(1): pp.1–13.
https://doi.org/10.1016/j.ymssp.2013.08.010

[22] Qin, Y., Xing, J., and Mao, Y. F. Weak transient fault feature extraction based on an optimized Morlet wavelet and kurtosis, *Measurement Science & Technology*, 2016, vol. **27**, no. 8, Art. no. 085003.
https://doi.org/10.1088/0957-0233/27/8/085003

[23] Wang, Y., Liu, D., Xu, G., et al., An image dimensionality reduction method for rolling bearing fault diagnosis based on singular value decomposition, *Proceedings of the Institution of Mechanical Engineers Part C Journal of Mechanical Engineering Science*, 2016, vol. **230**, no. 11, pp. 1830–1845.
https://doi.org/10.1177/0954406215585186

[24] Abdelkader, R., Kaddour, A., and Derouiche, Z. Enhancement of rolling bearing fault diagnosis based on improvement of empirical mode decomposition denoising method, *International Journal of Advanced Manufacturing Technology*, 2018, vol.**97**, no.13, pp.1–19.
https://doi.org/10.1007/s00170-018-2167-7

[25] Dragomiretskiy, K., Zosso, D. Variational mode decomposition . *IEEE Transactions on Signal Processing*, 2014, **62**(3): 531–544. https://doi.org/10.1109/TSP.2013.2288675

[26] Zhang, M., Jiang, Z. N., Feng, K. Research on variational mode decomposition in rolling bearings fault diagnosis of the multi-stage centrifugal pump. *Mechanical Systems and Signal Processing*, 2017, **93**: 460–493. https://doi.org/10.1016/j.ymssp.2017.02.013

[27] Noël, J.-P., Renson, L., Grappasonni, C., Kerschen, G. Identification of nonlinear normal modes of engineering structures under broadband forcing. *Mechanical Systems and Signal Processing*. 2016, **74**, 95–110. https://doi.org/10.1016/j.ymssp.2015.04.016

[28] Sun, H., Ren, A., Wang, Y., et al. Deformation and Vibration Analysis of Compressor Rotor Blades Based on Fluid-Structure Coupling. *Engineering Failure Analysis*, 2021, 122:105216. https://doi.org/10.1016/j.engfailanal.2021.105216

[29] Packard, N. H., Grutchfield, J. P., Farmer, J. D., et al. Geometry from a time series, *Phys Rev Lett*, 1980, **45**(9) 712–716. https://doi.org/10.1103/PhysRevLett.45.712

[30] Lin, J., Chen, Q. Fault diagnosis of rolling bearings based on multifractal detrended fluctuation analysis and Mahalanobis Distance Criterion. *Mechanical Systems and Signal Processing*, 2013, **38**(2): 515–533. https://doi.org/10.1016/j.ymssp.2012.12.014

[31] Yan, R., Gao, R. Complexity as a measure for machine health valuation. *IEEE Transaction Instrumentation and Measurement*, 2004, **53**(4):1327–1334. https://doi.org/10.1109/TIM.2004.831169

[32] Tang, Y. F., Liu, S. L., Liu, Y. H., et al. Fault diagnosis based on nonlinear complexity measure for reciprocating compressor. *Chinese Journal of Mechanical Engineering*, 2012,48(3): 102-107. https://doi.org/10.3901/JME.2012.03.102